CrystEngComm

Accepted Manuscript

ROYAL SOCIETY OF CHEMISTRY

www.rsc.org/crystengcomm

Cite this: DOI: 10.1039/c0xx00000x

www.rsc.org/xxxxxx

ARTICLE TYPE

Insights into the growth of small-sized SAPO-34 crystals synthesized by a vapor-phase transport method

Yicheng Zhang[a], Zhongyan Deng[a], Kake Zhu[a] and Xinggui Zhou*[a]

Received (in XXX, XXX) Xth XXXXXXXXX 20XX, Accepted Xth XXXXXXXXX 20XX

DOI: 10.1039/b000000x

Dry gel derived from a conventional hydrogel (or ultrasonically treated hydrogel) containing a low amount of tetraethylammonium hydroxide (TEAOH) was subjected to vapor-phase transport procedure using morpholine and produced SAPO-34 around 300-500 nm (or below 100 nm). The formation of small crystals is mainly benefited from the increase of tetra-coordinated Al atoms in dry gel promoted by heating and/or ultrasonic treatment.

Silicoaluminophosphate molecular sieve SAPO-34, with a **CHA** framework topology and medium/strong acidity, is an exceptional shape-selective catalyst for methanol-to-olefin (MTO) reaction [1,2]. However, its narrow windows of 8-ring restrict the efficient diffusion of intermediates and/or products out of the crystal usually with bulky size, leading to severe coke formation and fast deactivation [3]. Consequently, it is highly desirable to shorten the diffusion distance within the crystal. Principally, SAPO-34 nanocrystals [4-8] and hierarchical SAPO-34 [9-11] are the two kinds of target materials with enhanced mass-transfer properties.

Among the the previous studies, many methods focus on decreasing the crystal size of SAPO-34, which usually takes full advantage of the crystallization characteristics. Novel hydrothermal methods, such as colloidal solution method [5], mixed-templating strategy [7,12], post-synthesis milling and recrystallization method [8] and so on are competent of producing small-sized SAPO-34 crystals. Besides, dry gel conversion method is also frequently applied in the synthesis of SAPO-34, because it enjoys advantages over hydrothermal method including higher zeolite yield, less waste generation and smaller required reactor volume [13,14]. Volatile and non-volatile templates have been successfully applied for vapor-phase transport (VPT) and steam-assisted conversion (SAC) synthesis of SAPO-34, respectively. To obtain small-sized SAPO-34, polymer was applied to suppress the growth of SAPO-34 crystals during VPT crystallization [15]. In the case of SAC method, SAPO-34 crystals around 70 nm were obtained by using tetraethylammonium hydroxide (TEAOH) as a sole template [16]. However, this SAC method consumes a relatively high amount of the expensive TEAOH (TEAOH/Al_2O_3 = 1.8 or above) to complete crystallization, which impedes the wide application of the recipe and also results in difficult handling of sticky gel during preparation of dry gel (lump or powder). To avoid the demerits, we introduce a VPT method to crystallize SAPO-34 from a dry gel containing a low amount of TEAOH (TEAOH/Al_2O_3=1.0) with the aid of morpholine (MOR) in the vapor phase. The hydrogel is easy to be converted into a powder-like dry gel by heating thanks to the low content of TEAOH. The obtained SAPO-34 shows small size that facilitates MTO performance, and the crystal size can be further reduced by introducing ultrasonic technique into the VPT system, which increases the advantage of this method. To the best of our knowledge, this is the first reported case of employing both volatile MOR and non-volatile TEAOH as templates in the vapor-phase transport synthesis of SAPO-34. Moreover, we also elucidate the role of tetraethylammonium cation (TEA^+) in SAPO-34 crystallization by replacing the hydroxyl ion (OH^-) with bromine ion (Br^-).

When a dry gel contains a low amount of TEAOH (TEAOH / Al_2O_3 = 1.0), steam-assisted conversion of the dry gel produces a material (denoted as T-SAPO-34 (H)) with abundant amorphous phase, though with a little CHA phase (Fig. S1). Therefore, MOR as a second template is necessary for complete crystallization.

The synthesis parameters of samples are listed in Table S1. M-SAPO-34 (H) synthesized by VPT method from a template-free dry gel (TEAOH/Al_2O_3 = 0), which involves the vapor of the MOR and vapor of water, was used as a reference. TM-SAPO-34 (H) was synthesized by the VPT crystallization of dry gel containing a low amount of TEAOH (TEAOH/Al_2O_3 = 1.0). TM-SAPO-34 (US+H) has the additional step of ultrasonic treatment before the hydrogel was converted into dry gel by heating at 80 ^oC. H is short for heating (method of drying a hydrogel) and US is short for ultrasonic treatment.

As shown in Fig. S2, M-SAPO-34 (H) derived from template-free dry gel exhibits a rather bulky crystal size (about dozens of micrometers) and smooth face, similar to the MOR-templated SAPO-34 synthesized by hydrothermal method [12,17,18]. This verifies that MOR is good at accelerating the crystal growth of SAPO-34 and has little effect on the nucleation [17]. In the XRD pattern (Fig. 2a), M-SAPO-34 (H) exhibits a high intensity of typical CHA peaks, revealing the high specificity of MOR towards SAPO-34 phase in the VPT method [19]. Comparatively, TM-SAPO-34 (H) derived from TEAOH-templated dry gel exhibits a conspicuous reduction in crystal size (300-500 nm, Fig. 1a, b) and has correspondingly reduced intensity of XRD peaks (Fig. 2a). Although the added TEAOH is too few to fully crystallize SAPO-34 (T-SAPO-34 (H) in Fig. S1), its advantage,

namely generating nuclei, remains during VPT crystallization. Therefore, TEAOH and MOR display a synergistic effect on synthesizing small-sized SAPO-34. If the dry gel was derived from a ultrasonically treated hydrogel, the obtained TM-SAPO-34 (US+H) (Fig. 2a) is formed by aggregation of crystals smaller than 100 nm (Fig. 1c, d), which can be attributed to the enhanced generation of nuclei by US treatment. Although the XRD peak intensities of TM-SAPO-34 (H) and TM-SAPO-34 (US+H) are weaker than those of M-SAPO-34 (H) (Fig. 2a), they are not closely related to the observed crystal size, because the intergrowth of crystal will increase the intensity to different degrees.

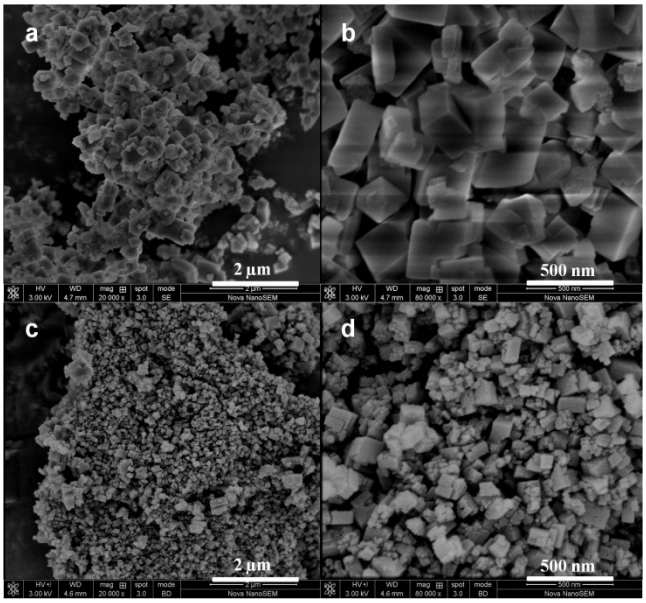

Fig. 1 SEM images of (a and b) TM-SAPO-34 (H) and (c and d) TM-SAPO-34 (US+H).

As shown in Fig. S3a, all the three materials display type-I N_2 adsorption-desorption isotherms. In addition, TM-SAPO-34 (H) and TM-SAPO-34 (US+H) show a steep increase of nitrogen adsorption at relatively high pressure ($P/P_0 > 0.9$), suggesting the existence of mesopores [8]. Compared with mesopore-free M-SAPO-34 (H), TM-SAPO-34 (H) possesses increased mesopore volume (0.16 cm^3g^{-1}), and TM-SAPO-34 (US+H) has a further increased value (0.21 cm^3g^{-1}), as tabulated in Table S2.

Under the same VPT condition, it is reasonable to attribute the formation of different-sized SAPO-34 to the state of dry gel associated with the preparation method. The dry gels for TM-SAPO-34 (H) and TM-SAPO-34 (US+H), *i.e.* DG (H) and DG (US+H), were prepared by heating (80 ^oC) the conventional hydrogel and ultrasonically treated hydrogel, respectively. For comparison, we also prepared a dry gel by using ethanol to dilute the conventional hydrogel followed by evaporating the solvent at ambient temperature. The dry gel was prepared without introducing any extra energy and is denoted as DG (E), where E represents ethanol and/or evaporation. The material crystallized from DG (E) is denoted as TM-SAPO-34 (E).

As shown in Fig. S4, TM-SAPO-34 (E) consists of crystal with size above 500 nm, larger than TM-SAPO-34 (H) (300-500 nm). As shown in the XRD patterns (Fig. 2b), all the three dry gels exhibit the characteristic peaks of bayerite phase at 2θ = 18.8, 20.3, 27.9 and 40.6^o (JCPDS 20–0011), together with a certain proportion of amorphous phase. Besides, DG (E) also contains oxonium aluminium oxide (2θ = 7.8 and 15.7^o, JCPDS 70–1204). FT-IR spectra of the dry gels exhibit no charactersitic peaks of T-O-T vibrational frequency of SAPO-34 lattice secondary building unit (SBU) at 635 and 530 cm^{-1} (Fig. S5)[20, 21]. The results of XRD and FT-IR prove that crystal nuclei of SAPO-34 is absent in the dry gels, that is, DG (H) and DG (US+H) is only at the induction stage of crystal nuclei. The absence of SAPO-34 phase in DG (US+H) (Fig. 2b) is different from the previously reported appearance of SAPO-34 after US treatment [22], probably because the former case uses an insufficient amount of TEAOH. In the ^{31}P MAS NMR spectra (Fig. 2c), DG (E) exhibits an additional peak at -19 ppm compared with DG (H) and DG (US+H), which implies the presence of layered structure [23]. In addition, the broad envelop between -25 – 0 ppm arises from many overlapping peaks and shows the presence of amorphous phase[23], demonstrating that the heating and/or US treatment destroy the vulnerable layered phase held by weak forces. There is no distinguishable ^{31}P signal difference between DG (H) and DG (US+H) to elucidate the different sizes of SAPO-34 (Fig. 2c). After crystallization, the representative sample TM-SAPO-34 (H) has the ^{31}P signal at -29 ppm corresponding to tetrahedral $P(OAl)_4$, and the one at -16 ppm is ascribed to $P(OAl)_x(H_2O)_y$, which is resulted from hydration of P atoms after a long-time exposure to moisture[24]. Similarly, ^{27}Al MAS NMR spectra in Fig. 2d shows that, besides a broader peak at 40 ppm assigning to tetra-coordinated Al, the crystalline TM-SAPO-34 (H) also displays an additional signal at -12 ppm, which is stemmed from hydration of the $Al(PO)_4$ species [24]. Furthermore, the abovementioned three dry gels also show the ^{27}Al signal at 40 ppm (denoted as P_{40}), suggesting the presence of tetra-coordinated Al before VPT crystallization. In addition, they exhibit another intensive signal at 6 ppm (denoted as P_6) corresponding to penta-coordinated Al [23]. The signal intensity ratio of P_{40} to P_6 follows the order of DG (US+H) > DG (H) > DG (E), consistent with the order of the size of the corresponding SAPO-34 crystals, *i.e.,* TM-SAPO-34 (E) > TM-SAPO-34 (H) > TM-SAPO-34 (US+H). The subtle but important difference highlights that the heating and/or US treatment help to perform a deeper transformation of penta-coordinated Al into tetra-coordinated Al in the dry gels (illustrated in Fig. 3), in line with the trend of coordination change during crystallization. This is contributable to generating more nuclei and thus forming small-sized SAPO-34 during the subsequent VPT crystallization. Certainly, the other characteristics of dry gels, including crystal phase (Fig. 2b) and phosphorus coordination (Fig. 2c), also contribute to the formation of small-sized SAPO-34, though with relatively uncertain behavior. Such an effect during the induction stage of crystal nuclei (dry gel preparation) is enhanced by heating, particularly by US treatment.

The state of template in the as-synthesized SAPO-34 was reflected by TGA and DTG in Fig. S6. Although without the participation of TEAOH, M-SAPO-34 (H) displays a larger weight loss than TM-SAPO-34 (H), indicating high incorporation of MOR molecules in M-SAPO-34 (H). Between 400-550 ^oC, TM-SAPO-34 (H) exhibits a steeper weight loss than M-SAPO-34 (H) (Fig. S6a), consistent with the sharper DTG peak at 420

°C of the former than that of the latter (Fig. S6b). This proves that TEAOH and MOR are both incorporated into the micropores and have the same decomposition temperature. Besides, TM-SAPO-34 (US+H) displays almost the same TGA and DTG curves as TM-SAPO-34 (H), because they have the same starting gel composition.

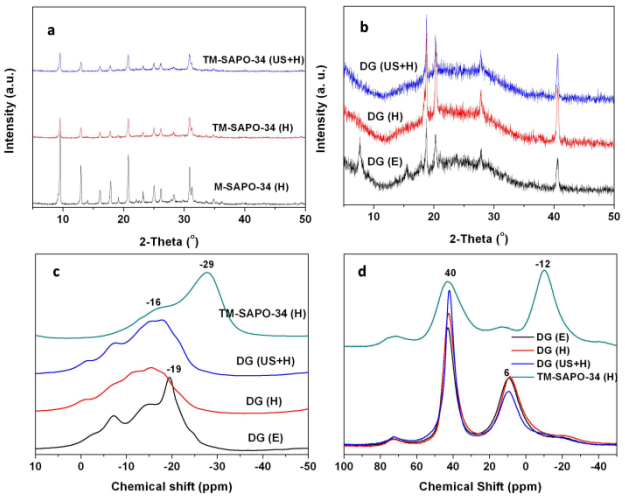

Fig. 2 (a) XRD patterns of M-SAPO-34 (H), TM-SAPO-34 (H) and TM-SAPO-34 (US+H); (b) XRD patterns of DG (E), DG (H) and DG (US+H); (c) ^{31}P MAS NMR spectra and (d) ^{27}Al MAS NMR spectra of DG (E), DG (H), DG (US+H) and TM-SAPO-34 (H).

^{29}Si MAS NMR spectra of the three materials are shown in Fig. S7. The highest peak is at -95.0 ppm assigned to Si(3Al) environment, because the high Si content in the dry gel results in a high number of framework Si atoms in the SAPO-34[25]. Correspondingly, the peak at -91.6 ppm assigned to $Si(OAl)_4$ species becomes the second intensive one. Pure silica islands are indicated by a signal at -110 ppm which is slightly present in the SAPO-34 samples. NH_3-TPD was employed to investigate the acidity of the three samples (Fig. S8). With the roughly similar acidic features, M-SAPO-34 (H) has relatively higher acidity amount than the other two samples, especially for strong acid sites (peak at around 440 °C).

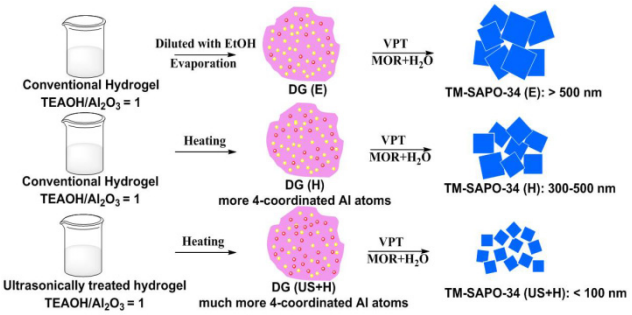

Fig. 3 Schematic diagram of synthesis of different-sized SAPO-34.

The MTO performance was tested on the three materials and is presented in Fig. S9 and Table S3. M-SAPO-34 (H) deactivates rapidly at initial period of reaction (10 min), due to the slow molecular diffusion in the large crystal. Comparatively, small-sized TM-SAPO-34 (H) has elongated catalytic lifetime of 270 min, though with earlier beginning time of deactivation at 170 min. With the smallest crystal size, TM-SAPO-34 (US+H) show the longest lifetime (330 min). The improved catalytic performance on the two nanosized catalysts reveals the beneficial impact of short diffusion length [26]. The steep decrease of methanol conversion after the beginning of deactivation (310 min) can be attributed to the close aggregation of crystals [6]. The selectivity to ethylene and propylene is very similar for the two small-sized SAPO-34 catalysts, which is higher than that of the rapidly deactivating M-SAPO-34 (H) (Fig. S9).

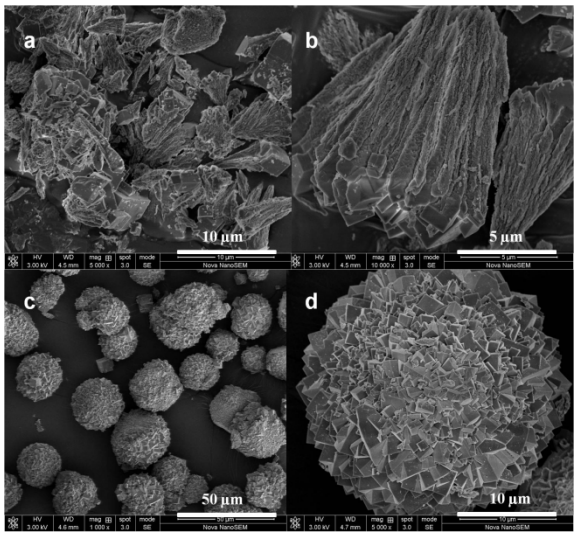

Fig. 4 SEM images of (a and b) Tb1M-SAPO-34 (H) and (c and d) Tb2M-SAPO-34 (H).

When TEAOH was substituted by equal molar amount of tetraethylammonium bromide (TEABr), the obtained Tb1M-SAPO-34 (H) also has reduced XRD peak intensity compared with M-SAPO-34(H) (Fig. S10), indicative of the reduction effect of TEABr on the crystal domains of SAPO-34. The morphology seems irregular (Fig. 4a), but a close observation on some particles shows a cone-like shape (Fig. 4b). Crystals with smooth surface and relatively regular shape are embedded on the bottom of the cone. When the addition amount of TEABr is doubled, the obtained Tb2M-SAPO-34 (H) remains good crystallinity (Fig. S10) but shows a very distinct morphology. Every particle has spherical morphology on which small and smooth-faced cubic crystals are embedded (Fig. 4c and d). The spherical Tb2M-SAPO-34 (H) is seemingly assembled from the cone-like crystals as possessed by Tb1M-SAPO-34 (H). The N_2 isotherms prove that the two materials possess improved mesoporosity compared with bulky M-SAPO-34 (H), but the mesoporosity is absolutely low (Fig. S11 and Table S4), from which we can infer the lack of voids within the spherical Tb2M-SAPO-34 (H). The NH_3-TPD profiles of Tb1M-SAPO-34 (H) and Tb2M-SAPO-34 (H) show a small proportion of strong acid sites (Fig. S12), similar to that reported by the previous research [27]. They exhibit short catalytic lifetimes of 30 and 50 min in MTO reaction (Fig. S13), respectively, both of which are slightly more stable than large-sized M-SAPO-34 (H) catalyst. However, the comparison between them and TM-SAPO-34 (H) facilitates the understanding of the role of TEA^+ in the VPT crystallization. The non-appearance of separate small-sized crystals suggests that TEABr alone can not serve as a template to promote nucleation or start

the crystallization for SAPO-34, due to the absence of OH^-, but indeed reduce the crystal domains. Despite this, the TEA^+ can be occluded in the micropores of Tb1M-SAPO-34 (H) and Tb2M-SAPO-34 (H), indicated by the sharper DTG peak (at 420 ^oC) than that of M-SAPO-34 (H) (Fig. S14b). However, doubled addition amount of TEABr renders a proportion of TEA^+ exposed on the external surface of Tb2M-SAPO-34 (H) (Fig. S14). In this case, it can be described that TEA^+ takes the role of a pseudo template in the VPT crystallization and inhibits the crystal growth.

Conclusion

Using morpholine in VPT method, small-sized SAPO-34 was crystallized from a dry gel containing a low amount of TEAOH template. A deeper transformation of penta-coordinated Al into tetra-coordinated Al in the dry gel was achieved by heating the hydrogel into dry gel, producing crystals with sizes between 300-500 nm. Additional US treatment upon the hydrogel could further strengthen this transformation and result in crystals below 100 nm in size. The couple of TEA^+ and OH^- is important to realizing the production of small-sized SAPO-34.

Acknowledgements

X. G. Zhou is grateful for financial support from the National Basic Research Program of China (2012CB720501) and the Natural Science Foundation of China (U1162112). K. K. Zhu is sponsored by New Century Excellent Talents in University (NCET-11-0644) of the Chinese Department of Education.

Notes and references

[a] *State Key Laboratory of Chemical Engineering, East China University of Science and Technology, Shanghai, 200237, P. R. China. E-mail: xgzhou@ecust.edu.cn*

† Electronic Supplementary Information (ESI) available: [details of any supplementary information available should be included here]. See DOI: 10.1039/b000000x/

[1] J. Q. Chen, A. Bozzano, B. Glover, T. Fuglerud and S. Kvisle, *Catal. Today*, 2005, **106**, 103-107.

[2] U. Olsbye, S. Svelle, M. Bjørgen, P. Beato, T. V. W. Janssens, F. Joensen, S. Bordiga and K. P. Lillerud, *Angew. Chem. Int. Edit.*, 2012, **51**, 5810-5831.

[3] D. Chen, K. Moljord and A. Holmen, *Microporous Mesoporous Mater.*, 2012, **164**, 239-250.

[4] H.-G. Jang, H.-K. Min, J. K. Lee, S. B. Hong and G. Seo, *Appl. Catal., A,* 2012, **437–438**, 120-130.

[5] H. van Heyden, S. Mintova and T. Bein, *Chem. Mater.,* 2008, **20**, 2956-2963.

[6] G. Yang, Y. Wei, S. Xu, J. Chen, J. Li, Z. Liu, J. Yu and R. Xu, *J. Phys. Chem. C*, 2013, **117**, 8214-8222.

[7] M. Sedighi, H. Bahrami and J. Towfighi Darian, *RSC Adv.*, 2014, **4**, 49762-49769.

[8] M. Yang, P. Tian, C. Wang, Y. Yuan, Y. Yang, S. Xu, Y. He and Z. Liu, *Chem. Commun.,* 2014, **50**, 1845-1847.

[9] F. Schmidt, S. Paasch, E. Brunner and S. Kaskel, *Microporous Mesoporous Mater.,* 2012, **164**, 214-221.

[10] F. Wang, L. Sun, C. Chen, Z. Chen, Z. Zhang, G. Wei and X. Jiang, *RSC Adv.*, 2014, **4**, 46093-46096.

[11] D. Xi, Q. Sun, J. Xu, M. Cho, H. S. Cho, S. Asahina, Y. Li, F. Deng, O. Terasaki and J. Yu, *J. Mater. Chem. A*, 2014, **2**, 17994-18004.

[12] Y.-J. Lee, S.-C. Baek and K.-W. Jun, *Appl. Catal., A*, 2007, **329**, 130-136.

[13] P. R. H. P. Rao, M. Matsukata, *Chem. Commun.,* 1996, 1441-1442.

[14] S. P. Naik, A. S. T. Chiang and R. W. Thompson, *J. Phys. Chem. B*, 2003, **107**, 7006-7014.

[15] J. Yao, H. Wang, S. P. Ringer, K.-Y. Chan, L. Zhang and N. Xu, *Microporous Mesoporous Mater.*, 2005, **85**, 267-272.

[16] Y. Hirota, K. Murata, S. Tanaka, N. Nishiyama, Y. Egashira and K. Ueyama, *Mater. Chem. Phys.,* 2010, **123**, 507-509.

[17] N. Nishiyama, M. Kawaguchi, Y. Hirota, D. Van Vu, Y. Egashira and K. Ueyama, *Appl. Catal., A*, 2009, **362**, 193-199.

[18] Q. Sun, N. Wang, D. Xi, M. Yang and J. Yu, *Chem. Commun.,* 2014, **50**, 6502-6505.

[19] L. Zhang, J. Yao, C. Zeng and N. Xu, *Chem. Commun.,* 2003, 2232-2233.

[20] A. K. Singh, R. Yadav and A. Sakthivel, *Microporous Mesoporous Mater.*, 2013, **181**, 166-174.

[21] J. Tan, Z. Liu, X. Bao, X. Liu, X. Han, C. He and R. Zhai, *Microporous Mesoporous Mater.*, 2002, **53**, 97-108.

[22] S. Askari, R. Halladj, *Ultrason. Sonochem.,* 2012, **19**, 554-559.

[23] L. Zhang, J. Bates, D. Chen, H.-Y. Nie and Y. Huang, *J. Phys. Chem. C*, 2011, **115**, 22309-22319.

[24] Z. Li, J. Martinez-Triguero, P. Concepcion, J. Yu and A. Corma, *Phys. Chem. Chem. Phys.,* 2013, **15**, 14670-14680.

[25] T. Álvaro-Muñoz, C. Márquez-Álvarez and E. Sastre, *Catal. Today*, 2012, **179**, 27-34.

[26] Q. Sun, Y. Ma, N. Wang, X. Li, D. Xi, J. Xu, F. Deng, K. B. Yoon, P. Oleynikov, O. Terasaki and J. Yu, *J. Mater. Chem. A*, 2014. 2, 17828-17839.

[27] Alvaro-Munoz, E. Sastre and C. Marquez-Alvarez, *Catal. Sci. Technol.*, 2014, **4**, 4330-4339.

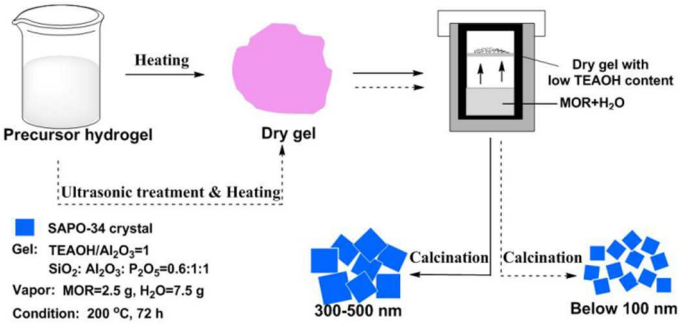

Under VPT conditions, a dry gel derived from a conventional hydrogel (or a ultrasonically treated hydrogel) can be converted into SAPO-34 crystals around 300-500 nm (or below 100 nm).